

Ground state energy and phase transitions of Long-range XXZ using VQE

Mrinal Dev* and Shraddha Sharma†

Department of Physics and Astronomy, National Institute of Technology Rourkela, Rourkela—769008, India

The variational quantum eigen solver (VQE), has been widely used to find the ground state energy of different Hamiltonians with no analytical solutions and are classically difficult to compute. In our work, we have for the first time used VQE to identify the phase transition boundary for an infinite order phase transition. Typically, in a finite order phase transition, finite-order derivatives of the ground state energy would signal the phase transition. However, this is not the case for the infinite order phase transitions, where a globally ranged order parameter is required. In this work, we use long-range XXZ (LRXXZ) chain for our study. It has been observed that there exist two types of phase transitions for this model. One of which is a first-order phase transition, straightforwardly evaluated by the gradient of the ground energy. Second, an infinite order phase transition, which is conventionally unfeasible to evaluate using the ground state energy. Therefore, it has been observed that the ground state energy is not sufficient to probe both of these transition boundaries. However, we propose a simple technique to utilise the ground state energy from VQE to identify both the phase transitions. The idea rests on the argument that VQE requires an ansatz circuit; therefore, the accuracy of the VQE will rely on this ansatz circuit. We have designed the ansatz circuit such that the estimated ground state energy is sensitive to the phase it is evaluated in. It is achieved by applying the constraint that the net spin remains constant throughout the optimization process. Consequently, the ansatz works in a certain phase where it gives relatively small random error, as it should, when compared to the error in ground state energy calculations of the other phases, where the ansatz fails. Identifying these changes in the behaviour of the error in ground state energy evaluation using VQE, we were able to identify the phase boundaries. Using exact diagonalisation, we also compare the behaviour of the energy gradient and energy gap across both the phase transition boundaries for this model. Further, by increasing the depth of the optimisation circuit, we also accurately evaluate the ground energy of the LRXXZ chain for the value of coupling constant, $J = -1$.

I. INTRODUCTION

Interacting many-electron systems have been at the forefront of condensed matter physics¹ and is pursued as an attempt to design and understand properties of useful materials² and also to understand fundamental science³. In this matter, studying long-range interactions has gained a lot of attraction in recent times because of the many emerging setups in atomic, molecular, and optical physics (AMO). There has also been several experimental improvements in the cooling, trapping, and controlling of many-body atomic and molecular quantum systems possessing long-range interactions^{4–7}. Theoretically, it has also been extensively studied in condensed matter physics^{8–10}. Although the short-range systems can be used to derive properties of their corresponding long-range interacting system (in the limiting case), many novel phenomena are exclusive to the long-range interaction itself^{4,11,12}. Experimentally, it has been possible to engineer 2D- Ising lattice with power-law decaying interaction between spins¹³. In the study of ultra-cold atoms, it has been observed that for fermionic and bosonic isotopes of Cr, Dy, and Er, a coherent spin-exchange has been induced by a large dipole-dipole interaction in the range of $\frac{1}{r^3}$ ^{14–19}.

In our work, we have evaluated the ground-state energy of the Long Range XXZ model (LRXXZ) with good accuracy and evaluated its phase transitions using quantum algorithms. Generally, phase transitions are usually studied using singularities or discontinuities in local variables

by varying these parameters along the critical point or using the two-point correlation function²⁰. These methods are sufficient for a finite-order phase transitions, however, such techniques fail when we have an infinite-order phase transition or a topological transition. These transitions are only accessible through global parameters²¹ and can usually only be accurately obtained by quantum Monte Carlo or density-matrix renormalization group methods^{22,23}. Entanglement properties can also be very useful in this domain, von Neumann entropy^{24–28} and geometric entanglement^{29–33} have been shown to be good candidates in detecting these quantum phase transitions. This domain of phase transitions is yet to be explored by quantum computing. In our work, we propose to use Variational Quantum Eigensolver (VQE) to probe different phase transitions of LRXXZ system. VQE is a very powerful algorithm for condensed matter physics and has been used to find the ground state energy of complex systems like the Fermi-Hubbard model³⁴. The VQE is conventionally designed to extract the ground state energy; using this technique, we also obtain the ground state energy of the LRXXZ chain with good accuracy.

II. LONG-RANGE XXZ MODEL

In this section, we will start with the introduction to our model under consideration, i.e., the long-range XXZ chain, given by the Hamiltonian,

$$H = -J \sum_{i \neq j}^N \frac{S_i^x S_j^x + S_i^y S_j^y + \Delta S_i^z S_j^z}{|i - j|^\alpha}, \quad (1)$$

where J is the coupling constant, Δ is the anisotropy term, whereas, $S^{x,y,z}$ are Pauli spin- $\frac{1}{2}$ operators. The i, j represents site indices, with $i \in \mathbb{Z}$ ($i \in [0, N]$, N being the system size), and the range of interaction is defined by α , with $\alpha \in \mathbb{R}$. When α is small, the system is long-range interacting, and as α tends to infinity, it transforms to the short-range XXZ model, implying only nearest-neighbor interaction. The one-dimensional short-range XXZ has been extensively studied³⁵ and its phases are well known. It was observed that for $J > 0$, the paramagnetic (PM) phase is obtained for $-1 < \Delta < 1$, whereas for $\Delta > 1$, the system is in the ferromagnetic (FM) phase, and for $\Delta < -1$ it is in the anti-ferromagnetic (AFM)³⁵ phase. However, as the range of interaction is increased, it has been observed that the transition point of AFM to PM phase starts to shift towards more negative Δ values. In contrast, the PM-FM transition point remains the same^{36,37}.

III. VQE AND THE ANSATZ CIRCUIT

The VQE is a hybrid quantum-classical method that can be used to find the ground-state energy of a Hamiltonian. The expectation value of the Hamiltonian is computed over a parameterized state using a quantum processor, while a classical optimizer adjusts the parameters to minimize energy³⁸. An ansatz state or a guess state is chosen for parameterization. We start initially with the Neel state, which is prepared by applying the Pauli- X gate alternatively to the initial default $|000 \dots\rangle$ state. The alternatively applied Pauli- X gates will flip $|0\rangle \rightarrow |1\rangle$, leaving us with $|1010 \dots\rangle$ Neel state as shown in Fig. (1). Once the $|1010 \dots\rangle$ is obtained, we apply parameterized gates, as shown in Fig. (2), leading to our ansatz state. Afterwards, we tune the parameters of these gates to minimize energy, which leads the guess state closer and closer to the actual ground state of the system. In simple terms, through the circuit shown in Fig. (2), we make a guess at a ground state i.e., the parameterized state. Thereafter, we vary the parameters until the ground state is reached by minimizing the energy. We can construct our ansatz circuit such that the total spin remains constant throughout. This approach, combined with the choice of the initial state, will play a crucial role in finding phase transitions, as we will see later in the paper.

It is therefore clear that this approach heavily relies on the initial guess for our ground state or the ansatz state. The better our guess is, the easier we can reach the ground state. There are several good guesses; one of them is the HVA (Hamiltonian variational ansatz). In HVA, one constructs the ansatz using the Hamiltonian

of the system; every term is written in the form of Pauli matrices, and the matrix representation of these terms can be found. Then, these matrices can be implemented using the gates one wishes to use, depending on the hardware of the system. These gates are parameterized, and all terms that commute share parameters as they have the same eigenstate. For the short-range XXZ Hamiltonian, the ansatz is constructed by separating it into odd and even parts; all the odd parts and even parts are disjoint from each other, so they commute with each other and can be run in parallel with the same parameter³⁹. The Hamiltonian can be separated in the following way

$$\begin{aligned} H^{\text{even}} &= \sum_s H_{ss}^{\text{even}} = \sum_s \sum_{i=1}^{N/2} \sigma_{2i-1}^s \sigma_{2i}^s, \\ H^{\text{odd}} &= \sum_s H_{ss}^{\text{odd}} = \sum_s \sum_{i=1}^{N/2-1} \sigma_{2i}^s \sigma_{2i+1}^s, \end{aligned} \quad (2)$$

where $s \in \{x, y, z\}$ denotes the spin component. Each of the spins has different parameters, but each even bond and each odd bond will have the same parameter because they are disjoint. For $N = 4$,

$$\begin{aligned} \text{Even bonds: } (1, 2), (3, 4) &\rightarrow \sum_{s \in x, y, z} (\sigma_1^s \sigma_2^s + \sigma_3^s \sigma_4^s). \\ \text{Odd bonds: } (2, 3) &\rightarrow \sum_{s \in x, y, z} (\sigma_2^s \sigma_3^s). \end{aligned}$$

We can put all the terms in a single equation representing the implementation of the ansatz circuit as:

$$\begin{aligned} U_{XXZ}(\beta, \gamma, \theta) &= \prod_{\ell=1}^p G(\theta_\ell, H_{zz}^{\text{odd}}) G(\theta_\ell, H_{zz}^{\text{even}}) \\ &\quad \times G(\gamma_\ell, H_{xx}^{\text{odd}}) G(\gamma_\ell, H_{xx}^{\text{even}}) \\ &\quad \times G(\beta_\ell, H_{yy}^{\text{odd}}) G(\beta_\ell, H_{yy}^{\text{even}}), \end{aligned} \quad (3)$$

$$\text{with, } G(\theta, H) = e^{-i\theta H/2} \quad (4)$$

Like HVA, we have also used the Hamiltonian for our inspiration to construct the circuit. In the variational ansatz, the Hamiltonian is decomposed into even and odd parts, and these parts are parameterized separately. We have used a different approach to construct the ansatz. Let us first look at our Hamiltonian:

$$e^{-iHt} \rightarrow e^{-it(S_i^x S_{i+1}^x + S_i^y S_{i+1}^y + \Delta S_i^z S_{i+1}^z)} \quad (5)$$

Since $[S_i^x S_{i+1}^x + S_i^y S_{i+1}^y, S_i^z S_{i+1}^z] = 0$, we can write:

$$e^{-it(S_i^x S_{i+1}^x + S_i^y S_{i+1}^y + \Delta S_i^z S_{i+1}^z)} = e^{-i\theta(S_i^x S_{i+1}^x + S_i^y S_{i+1}^y)} e^{-i\phi S_i^z S_{i+1}^z} \quad (6)$$

We parameterize time with θ and ϕ . Since we know the matrix representation of $S^{s \in \{x, y, z\}}$, we can use them to

find the matrix representation of each part as:

$$e^{-i\theta(S_i^x S_{i+1}^x + S_i^y S_{i+1}^y)} e^{-i\phi S_i^z S_{i+1}^z} = \begin{bmatrix} 1 & 0 & 0 & 0 \\ 0 & \cos \theta & -i \sin \theta & 0 \\ 0 & -i \sin \theta & \cos \theta & 0 \\ 0 & 0 & 0 & 1 \end{bmatrix} \times \begin{bmatrix} e^{-i\phi} & 0 & 0 & 0 \\ 0 & e^{i\phi} & 0 & 0 \\ 0 & 0 & e^{i\phi} & 0 \\ 0 & 0 & 0 & e^{-i\phi} \end{bmatrix}. \quad (7)$$

We further show in Eqs. (8) and (9) the circuit implementation for these matrices.

$$\begin{bmatrix} 1 & 0 & 0 & 0 \\ 0 & \cos \theta & -i \sin \theta & 0 \\ 0 & -i \sin \theta & \cos \theta & 0 \\ 0 & 0 & 0 & 1 \end{bmatrix} \rightarrow \begin{array}{c} q_0 \text{ --- } \bullet \text{ --- } \boxed{R_x(\theta)} \text{ --- } \bullet \text{ ---} \\ | \quad | \quad | \quad | \\ q_1 \text{ --- } \oplus \text{ --- } \bullet \text{ --- } \oplus \text{ ---} \end{array} \quad (8)$$

$$\begin{bmatrix} e^{-i\phi} & 0 & 0 & 0 \\ 0 & e^{i\phi} & 0 & 0 \\ 0 & 0 & e^{i\phi} & 0 \\ 0 & 0 & 0 & e^{-i\phi} \end{bmatrix} \rightarrow \begin{array}{c} q_0 \text{ --- } \bullet \text{ --- } \boxed{R_z(\theta)} \text{ --- } \bullet \text{ ---} \\ | \quad | \quad | \quad | \\ q_1 \text{ --- } \oplus \text{ --- } \bullet \text{ --- } \oplus \text{ ---} \end{array} \quad (9)$$

Afterwards, these gates are applied to all the qubits in the system, connecting each of the neighbouring qubits, which makes just 1 layer of the circuit (depth=1). The ansatz circuit is repeated upto the desired depth (=2, in our case). However, after implementation we found that the ansatz circuit did not achieve the ground state very effectively, so we modified the RZ gate with the CRZ gate. These modifications are allowed because the ansatz circuit is just a guess circuit for finding the ground state energy and need not follow any particular rule, and the guess that works the best may be chosen. The final ansatz circuit after the application of an alternate X -gate is represented in Fig. (2).

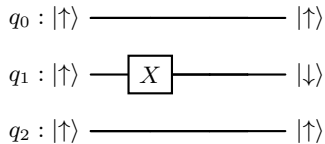


FIG. 1: Circuit representation of initialisation using three-qubits with alternate application of the X -gate.

We have parameterized every single gate with a different parameter. This is unlike conventional variational ansatz, where commuting terms share the same parameters; however, doing this allows us to achieve the expected ground state energies with very low circuit depth of $p = 2$, compared to previous studies³⁹. Through this method, we find the number of parameters required in total is $4N$, *i.e.* $2N$ parameters per layer. Conventionally, an even-odd variational ansatz has $2N$ parameters, for example, the XXZ model requires 4 parameters per

layer with $N/2$ total layers. However, our circuit has a much lower circuit depth, so the number of gates required is also much less comparatively. The number of gates is equal to the number of parameters, but for HVA, the number of gates can be multiple times the number of parameters. The main advantage is that it works efficiently with LRXXZ as well.

We have not only used this method to find the ground state energy of LRXXZ efficiently for $J < 0$, but also, for the first time, used a quantum algorithm to explore the long-range phase transitions for the case of $J > 0$. In order to do this, we exploited our initial state coupled with the fact that the ansatz circuit is designed in a way that it does not cause the net magnetization to change. We evaluated the error between the ground state energy obtained via exact diagonalization and the energy evaluated by VQE. The error evaluated from this method showed dependency on the phase in which it was evaluated. We exploited this feature to mark the phase transitions. We will take a closer look at these methods in the results section.

IV. RESULTS

In this section, we provide the details of our novel scheme to probe different phase transitions in the LRXXZ model. In Sec. (IV A), utilizing directional coherence, we probe the phase transition boundaries between FM-PM and PM-AFM phases and compare the two phase transitions. Furthermore, in Sec. (IV B) we also present our results of VQE for depth= 2, $J = -1$, and plot the relative error for the whole phase diagram.

We start our discussion by introducing the idea of directional coherence as a useful probe for detecting phase transitions.

A. Phase Transition of Long-Range XXZ chain

We start by analysing the energy difference of the exact diagonalisation results and the ground energy computed through VQE ($E_d(\Delta, \alpha) = E_{exact} - E_{VQE}$) at depth 1 as a function of Δ and α . The depth is chosen to be 1 because, in this section, our goal was to obtain phase transitions rather than to achieve ground energy with accuracy. We further computed the gradient of this energy difference along α and Δ , and utilized it to compute normalized gradient vectors represented as arrows in our phase diagrams. The components of these gradient vectors for each Δ and α can be calculated as:

$$u_x = \frac{\partial E_d / \partial \alpha}{\sqrt{(\partial E_d / \partial \alpha)^2 + (\partial E_d / \partial \Delta)^2}} \\ u_y = \frac{\partial E_d / \partial \Delta}{\sqrt{(\partial E_d / \partial \alpha)^2 + (\partial E_d / \partial \Delta)^2}}. \quad (10)$$

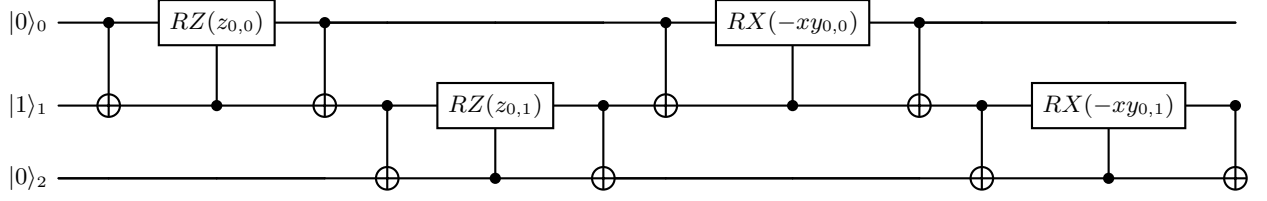


FIG. 2: Three-qubit ansatz circuit for a single layer.

The main objective in calculating the gradient vector is to finally obtain the information of *directional coherence*. For this purpose, we obtain the angle of the gradient vector, as:

$$\theta = \tan^{-1}(u_y/u_x). \quad (11)$$

The directional coherence, then, has been calculated as:

$$\text{Directional coherence} = \sqrt{\tilde{\sin}^2 \theta + \tilde{\cos}^2 \theta} \quad (12)$$

where, $\tilde{\sin} \theta$, $\tilde{\cos} \theta$, are the means of $\sin \theta$, $\cos \theta$, over a moving window. The size of the moving window has been varied to get a smooth and accurate result.

The idea is that the ansatz state works particularly well in one phase, leading to a random lower value of E_d , and therefore, E_d is expected to be lower in one phase as compared to that in the other phase. The directional coherence, therefore, helps differentiate between the regions where the nature of the E_d changes is owing to the underlying phase transition. Graphically, directional coherence represents the behaviour of arrows in a particular region. We exploit the pattern in the orientation of these arrows. As an example, we observe that these arrows representing gradient vectors point randomly in one phase (AFM), whereas it shows a systematic pattern in another phase (PM/FM). The directional coherence can capture this change in the behaviour of arrows, not only between a random or systematic orientation but also between two systematic orientations in two different directions. This is evident in our phase diagrams where we have overlaid the arrows on the pseudo-colour plots of the directional coherence (Fig. (3a) and (4a)). We observed that the direction of these arrows can be understood and is in compliance to a good extent with the existing mean field results³⁶. For the subsequent subsections, we will consider $J = 1$.

1. FM to PM phase

For comparison, we explore the behaviour of the energy gap (between the ground and the first-excited state) and the gradient of the ground state energy. These are excellent indicators of any phase transition. The gradient has been computed by finding the exact ground state energy using the exact diagonalisation technique and taking the

derivative along Δ and α as shown in Fig. (3b). The Fig. (3b) shows the transition from the PM phase to the FM phase at -1 ³⁷. Left of $\Delta = -1$ is the PM phase, and right of it is the FM phase. This transition at $\Delta = -1$ can be observed in Fig. (3b), depicting the gradient of the ground state energy, and in Fig. (3c) representing the energy gap. It can also be observed from Fig. (3a) that this PM-FM transition can also be probed using the directional coherence. In Fig. (3a), we present the behaviour of directional coherence over the whole phase diagram overlaid by gradient vectors. It was observed that the direction of arrows change abruptly from PM phase ($\Delta < -1$) to the FM phase ($\Delta > -1$). Consequently, we see a strip in this region in the directional coherence phase diagram, indicating a phase transition. One can also comment crudely on the direction of arrows using mean-field theory³⁶ in the FM phase. The energy difference, E_d in this case can be represented as

$$E_d = |(E_{\text{FM}})_{\text{exact}} - (E_{\text{AFM}})_{\text{approx}}| \approx |(E_{\text{FM}})_{\text{MF}} - (E_{\text{AFM}})_{\text{MF}}|, \quad (13)$$

where, E_{FM} and E_{AFM} are energies for the FM and AFM phases, respectively. The subscript *approx* is added to reflect that for depth=1, the actual ground state energy in AFM phase can be slightly different from the one obtained from VQE. However, from the mean-field point of view, we can approximate E_d as the difference between the energies in the FM and AFM phases. The reason E_d is taken to be the difference between the E_{FM} and E_{AFM} is because the ansatz is chosen such that the energy obtained from VQE will be very close to that of the AFM phase (for depth-1), whereas the exact diagonalization would lead to E_{FM} . Proceeding in the same line of arguments as in Ref. [36], E_d for the case of FM phase will be:

$$E_d = \frac{|\Delta|}{4} \left| \sum_{\substack{i,j \\ i \neq j}} \left(\frac{1}{|i-j|^\alpha} \right) - \frac{\epsilon_i \epsilon_j}{|i-j|^\alpha} \right|, \quad (14)$$

where, $\epsilon_i = 1(-1)$ for $i \in \text{even}(\text{odd})$. Therefore, as α is increased, the overall E_d will decrease, but as Δ is a multiplying factor, the arrows will deviate in the increasing direction of Δ . To summarize, we started with an AFM state in the z -direction and used a circuit that kept

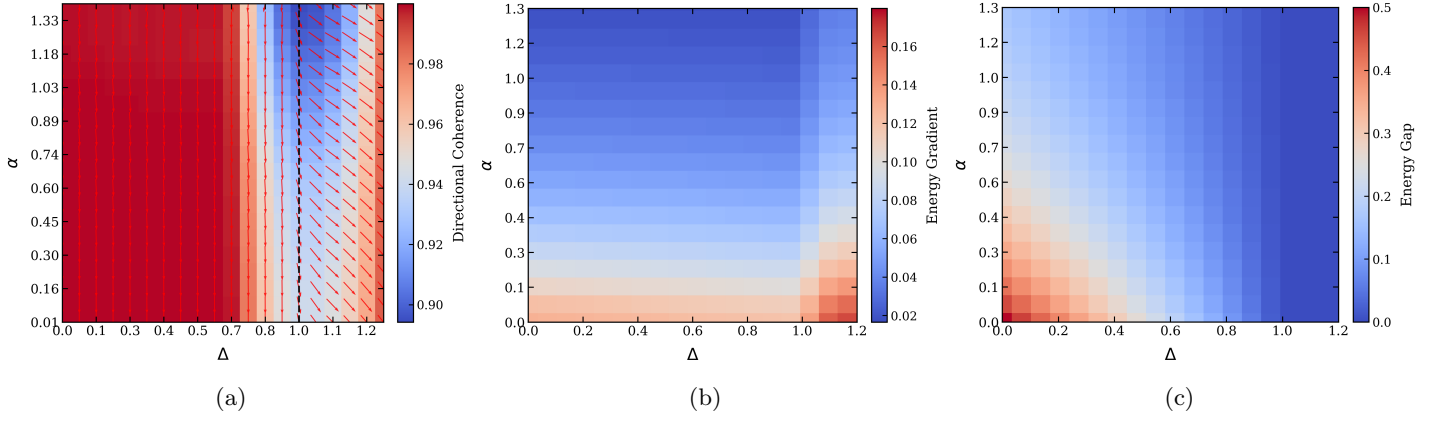


FIG. 3: Phase diagram of (a) directional coherence, (b) ground state energy gradient, and (c) energy gap. In (a) a dotted line is plotted at the point where the direction of arrow changes, directly coinciding with $\Delta = -1$, which marks the phase transition from PM phase to the FM phase.

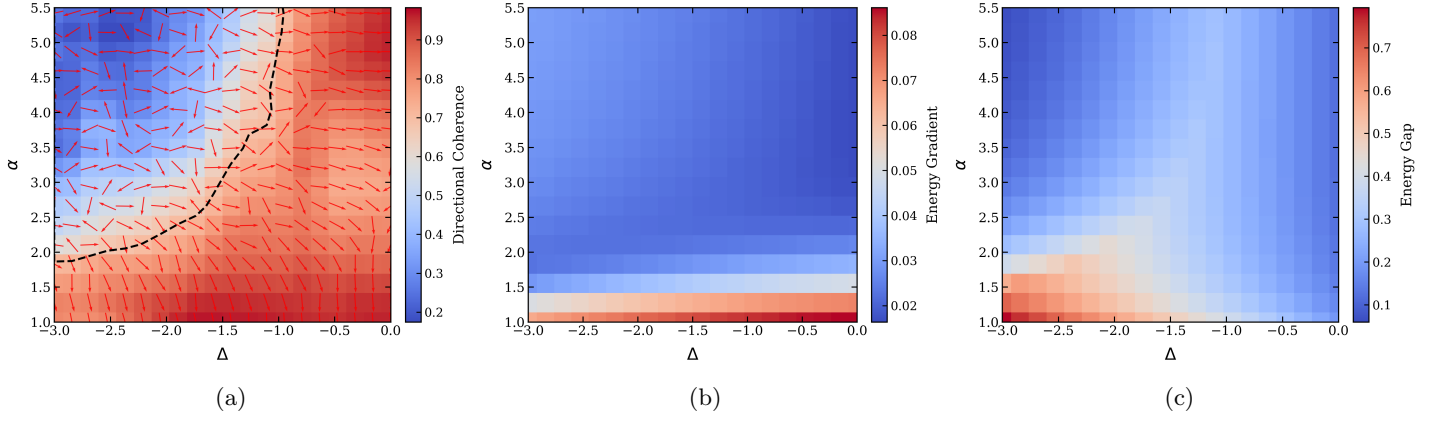


FIG. 4: Phase diagram of (a) directional coherence, (b) energy gradient, and (c) energy gap, as a function of Δ and α shows the clear depiction of AFM-PM phase transition in (a) as compared to (b) and (c). The dotted line in (a) separates the region of randomly oriented arrows (AFM phase depicted by blue region) with respect to the organised region (PM phase shown in red).

the net magnetization zero in the z -direction. Therefore, our algorithm will never reach FM ground energy and will miserably fail because it will always stay in the zero magnetization state and, which leads to an increase in the error abruptly. The error will increase as Δ increases, and the arrows will start to point toward the positive Δ direction. This is a first-order transition, and its clear identification using our technique of directional coherence is a direct consequence of the initial state we started with.

2. Paramagnetic phase to AFM phase

Now we will be looking at a more complicated phase transition of infinite order. Fig. 4 shows a phase transition from the PM phase in the right to the AFM phase in the top left corner. This phase transition is also visible in the pseudo-colour plot of the directional coherence

and is a consequence of our initial ansatz state, which is an AFM state. Now, in the PM phase, the net magnetisation is still zero, but the AFM order is absent and is more disordered. Our optimizer can still get to the ground state, but since we started with an ordered AFM phase, it is easier for the optimizer to find the ground state in the AFM region than in PM region. However, it still reaches some energy minima, which, as compared to the case of FM phase, is impossible with the same initial ansatz state. Therefore, the increase in error is maximum and abrupt when transitioning to FM from PM phase. However, this change in E_d is gradual during the transition from the AFM to the PM phase. Since this change in error is not very suitable in AFM-PM phase transition case, we evaluated the gradient of the energy difference at the each point and found it to be randomly aligned in the AFM region and aligned in some particular direction in the PM region. Consequently, we found the direction coherence of the gradient that sepa-

rated the region with a random direction gradient from the region where the gradients were aligned in a particular direction. This allowed us to obtain a clear phase boundary between the two regions, Fig. (4a). This aligns perfectly with previously obtained phase transitions with geometric entanglement³⁷. The Ref. [37] has used an inverse α value, so the transition at $\Delta = -3$ is at inverse $1/\alpha \approx 0.56$, which corresponds to $\alpha \approx 1.78$. In our case, we find the critical α to be equal to 1.75. However, as shown in Fig. (4b), this phase transition is not at all identifiable in the gradient phase diagram since it is an infinite order phase transition. Although it is possible to observe it faintly in the energy gap phase diagram in Fig. (4c), it is not very accurate, and even for that, one needs to find the excited state energy.

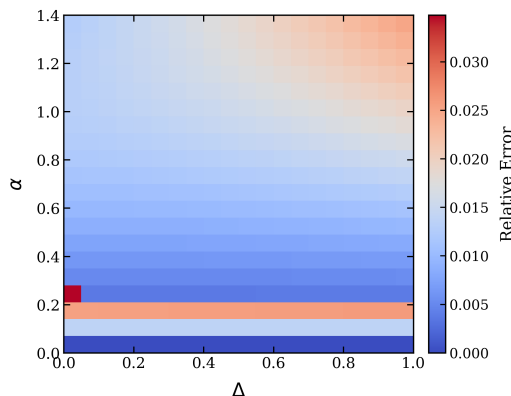


FIG. 5: The plot of relative error of VQE energy with respect to the exact diagonalization in the PM phase of LRXXZ with $J = -1$.

B. Depth 2

In this section, depth 2 has been employed to accurately determine the ground state energy. In the previous section, we used the error in the VQE algorithm (with respect to the actual ground state), to study different phases of LRXXZ, but in fact we can also use the same ansatz circuit at a higher depth to find the ground state energy more accurately. In this case, we have taken $J < 0$, for some unknown reason, changing the sign gave

us a better ground state energy when evaluated using VQE. The ansatz circuit is the same as previously shown in Fig. (9). A strategy for faster convergence is used, where the parameters of the ground state energy at one point have been passed on to the next point as the initial parameters for the next, and so on. We have used the Coby optimiser with 4000 iterations. The Fig. (5) shows that the maximum relative error is around 0.03, which is around 3% and the minimum relative error is 0. This reflects that our VQE works well for a wide range of parameters, even in depth 2, which has never been reported in previous studies^{39,40}

V. CONCLUSION

In this paper, we have shown that the VQE approach is not just limited to finding the ground state energy of a system, but can be used to identify phase transitions of model Hamiltonians, which are rather difficult to identify. We have been able to clearly identify both first-order and infinite order phase transitions for the LRXXZ model, using the difference between the exact ground state energy and the ground state energy evaluated via VQE, referred to as the error in energy. We observe that the gradient vector of the error showed a clear distinction between different phases. Their behaviour and direction are in compliance with the mean-field approach. This method is advantageous as it only requires us to find the ground state energy. Achieving an infinite order phase transition using the ground state energy may seem counterintuitive and impossible, but through this method, it has been demonstrated to be achievable. This method can be further utilised to identify other transitions where the ground state symmetries change across the transition boundary. Depending upon the type of system and transitions, one may design their ansatz to suit the problem, and therefore, it opens up a completely new approach to identifying phase transitions.

VI. ACKNOWLEDGMENTS

Shraddha Sharma acknowledges the financial support from the Department of Science and Technology (DST), Government of India, through the DST-INSPIRE Faculty Fellowship (DST/INSPIRE/04/2023/00184; Faculty Registration No. IFA23-PH303)

* mrinaldev3@gmail.com

† sharmas@nitrrkl.ac.in, shrdha1987@gmail.com

¹ J. P. LeBlanc, A. E. Antipov, F. Becca, I. W. Bulik, G. K.-L. Chan, C.-M. Chung, Y. Deng, M. Ferrero, T. M. Henderson, C. A. Jiménez-Hoyos, *et al.*, Physical Review X **5**, 041041 (2015).

² D. J. Scalapino, Reviews of Modern Physics **84**, 1383 (2012).

³ D. P. Arovas, E. Berg, S. A. Kivelson, and S. Raghu, Annual review of condensed matter physics **13**, 239 (2022).

⁴ T. Lahaye, C. Menotti, L. Santos, M. Lewenstein, and T. Pfau, Reports on Progress in Physics **72**, 126401 (2009).

⁵ C. Schneider, D. Porras, and T. Schaetz, Reports on Progress in Physics **75**, 024401 (2012).

⁶ C. Monroe, W. Campbell, E. Edwards, R. Islam, D. Kafri, S. Korenblit, A. Lee, P. Richerme, C. Senko, and J. Smith, "Ion traps for tomorrow's applications, proceedings of the

- international school of physics “enrico fermi,” course 189,” (2014).
- ⁷ A. Browaeys, D. Barredo, and T. Lahaye, *Journal of Physics B: Atomic, Molecular and Optical Physics* **49**, 152001 (2016).
 - ⁸ I. Bloch, J. Dalibard, and W. Zwerger, *Reviews of modern physics* **80**, 885 (2008).
 - ⁹ I. Bloch, J. Dalibard, and S. Nascimbene, *Nature Physics* **8**, 267 (2012).
 - ¹⁰ M. Lewenstein, A. Sanpera, and V. Ahufinger, *Ultracold Atoms in Optical Lattices: Simulating quantum many-body systems* (Oxford University Press (UK), 2012).
 - ¹¹ B. Spivak and S. A. Kivelson, *Physical Review B—Condensed Matter and Materials Physics* **70**, 155114 (2004).
 - ¹² D. Peter, S. Müller, S. Wessel, and H. P. Büchler, *Physical review letters* **109**, 025303 (2012).
 - ¹³ J. W. Britton, B. C. Sawyer, A. C. Keith, C.-C. J. Wang, J. K. Freericks, H. Uys, M. J. Biercuk, and J. J. Bollinger, *Nature* **484**, 489 (2012).
 - ¹⁴ A. De Paz, A. Sharma, A. Chotia, E. Marechal, J. Huckans, P. Pedri, L. Santos, O. Gorceix, L. Vernac, and B. Laburthe-Tolra, *Physical review letters* **111**, 185305 (2013).
 - ¹⁵ B. Naylor, A. Reigue, E. Maréchal, O. Gorceix, B. Laburthe-Tolra, and L. Vernac, *Physical Review A* **91**, 011603 (2015).
 - ¹⁶ M. Lu, N. Q. Burdick, S. H. Youn, and B. L. Lev, *Phys. Rev. Lett.* **107**, 190401 (2011).
 - ¹⁷ S. Baier, M. J. Mark, D. Petter, K. Aikawa, L. Chomaz, Z. Cai, M. Baranov, P. Zoller, and F. Ferlaino, *Science* **352**, 201 (2016).
 - ¹⁸ K. Aikawa, A. Frisch, M. Mark, S. Baier, R. Grimm, and F. Ferlaino, *Physical review letters* **112**, 010404 (2014).
 - ¹⁹ K. Baumann, C. Guerlin, F. Brennecke, and T. Esslinger, *nature* **464**, 1301 (2010).
 - ²⁰ S. Sachdev, *Physics world* **12**, 33 (1999).
 - ²¹ G. D. Chiara and A. Sanpera, *Rep. Prog. Phys.* **81**, 074002 (2018).
 - ²² D. M. Ceperley, *Rev. Mod. Phys.* **67**, 279 (1995).
 - ²³ U. Schollwöck, *Ann. Phys.* **326**, 96 (2011).
 - ²⁴ G. Vidal, J. I. Latorre, E. Rico, and A. A. Kitaev, *Phys. Rev. Lett.* **90**, 227902 (2003).
 - ²⁵ M. B. Hastings, *J. Stat. Mech.: Theory Exp.*, P08024 (2007).
 - ²⁶ P. Calabrese and J. Cardy, *J. Stat. Mech.: Theory Exp.*, P06002 (2004).
 - ²⁷ C. Holzhey, F. Larsen, and F. Wilczek, *Nucl. Phys. B* **424**, 443 (1994).
 - ²⁸ V. E. Korepin, *Phys. Rev. Lett.* **92**, 096402 (2004).
 - ²⁹ H. Barnum and N. Linden, *J. Phys. A: Math. Gen.* **34**, 6787 (2001).
 - ³⁰ A. Shimony, *Ann. N.Y. Acad. Sci.* **755**, 675 (1995).
 - ³¹ T.-C. Wei and P. M. Goldbart, *Phys. Rev. A* **68**, 042307 (2003).
 - ³² T.-C. Wei, D. Das, S. Mukhopadhyay, S. Vishveshwara, and P. M. Goldbart, *Phys. Rev. A* **71**, 060305(R) (2005).
 - ³³ R. Orús, *Phys. Rev. Lett.* **100**, 130502 (2008).
 - ³⁴ S. Stanisic, J. L. Bosse, F. M. Gambetta, R. A. Santos, W. Mroczkiewicz, T. E. O’Brien, E. Ostby, and A. Montanaro, *Nature communications* **13**, 5743 (2022).
 - ³⁵ F. Franchini *et al.*, *An introduction to integrable techniques for one-dimensional quantum systems*, Vol. 940 (Springer, 2017).
 - ³⁶ I. Frérot, P. Naldesi, and T. Roscilde, *Physical Review B* **95**, 245111 (2017).
 - ³⁷ J. Schneider, S. Thomson, and L. Sanchez-Palencia, *Physical Review B* **106**, 014306 (2022).
 - ³⁸ M. Cerezo, K. Sharma, A. Arrasmith, and P. J. Coles, *npj Quantum Information* **8**, 113 (2022).
 - ³⁹ R. Wiersema, C. Zhou, Y. de Sereville, J. F. Carrasquilla, Y. B. Kim, and H. Yuen, *PRX quantum* **1**, 020319 (2020).
 - ⁴⁰ J. Wang and R. Jaiswal, *arXiv preprint arXiv:2308.12020* (2023).